INTERNATIONAL JOURNAL FOR NUMERICAL METHODS IN FLUIDS
Int. J. Numer. Meth. Fluids 2005; **48**:1001–1021
Published online 7 April 2005 in Wiley InterScience (www.interscience.wiley.com). DOI: 10.1002/fld.973

Solution of the planar Newtonian stick–slip problem with the singular function boundary integral method

M. Elliotis[1], G. Georgiou[1,*,†] and C. Xenophontos[2]

[1]*Department of Mathematics and Statistics, University of Cyprus, P.O. Box 20537, 1678 Nicosia, Cyprus*
[2]*Department of Mathematical Sciences, Loyola College, 4501 N. Charles Street, Baltimore, MD 21210, U.S.A.*

SUMMARY

A singular function boundary integral method (SFBIM) is proposed for solving biharmonic problems with boundary singularities. The method is applied to the Newtonian stick–slip flow problem. The streamfunction is approximated by the leading terms of the local asymptotic solution expansion which are also used to weight the governing biharmonic equation in the Galerkin sense. By means of the divergence theorem the discretized equations are reduced to boundary integrals. The Dirichlet boundary conditions are weakly enforced by means of Lagrange multipliers, the values of which are calculated together with the singular coefficients. The method converges very fast with the number of singular functions and the number of Lagrange multipliers, and accurate estimates of the leading singular coefficients are obtained. Comparisons with the analytical solution and results obtained with other numerical methods are also made. Copyright © 2005 John Wiley & Sons, Ltd.

KEY WORDS: biharmonic equation; boundary singularity; Stokes flow; stick–slip problem; Lagrange multipliers; singular coefficients

1. INTRODUCTION

In the past few decades, many different numerical methods have been proposed for the treatment of boundary singularities in plane elliptic boundary value problems, in order to improve the solution accuracy and resolve the convergence difficulties occurring in the neighbourhood of such singular points. These methods range from special mesh-refinement schemes to sophisticated techniques that incorporate, directly or indirectly, the form of the local asymptotic expansion, which is known in many occasions. An exhaustive survey of treatment of singularities in elliptic boundary value problems is provided in the recent articles by Li and Lu [1], Dosiyev [2] and Shi *et al.* [3]. Knowledge of the coefficients appearing in the local solution expansion is often desired in many engineering applications. These coefficients, referred to as

*Correspondence to: G. Georgiou, Department of Mathematics and Statistics, University of Cyprus, P.O. Box 20537, 1678 Nicosia, Cyprus.
†E-mail: georgios@ucy.ac.cy

Received 25 October 2004
Revised 28 February 2005
Accepted 7 March 2005

singular coefficients or *generalized stress intensity factors* [4], are calculated either directly (see Reference [5] and references therein) or by post-processing the numerical solution [6, 7].

In the past few years, we have developed the singular function boundary integral method (SFBIM) for Laplacian problems with boundary singularities [5, 8, 9], in which the unknown singular coefficients are calculated directly. The solution is approximated by the leading terms of the local asymptotic solution expansion which are also used to weight the governing equation in the Galerkin sense. With a double application of Green's theorem, the discretized equations are reduced to boundary integrals over those parts of the boundary that do not involve the singular point. The Dirichlet boundary conditions are weakly enforced by means of Lagrange multipliers, which are calculated simultaneously with the singular coefficients. The method has been tested on standard Laplacian problems, yielding extremely accurate estimates of the leading singular coefficients, and exhibiting exponential convergence with respect to the number of singular functions [5, 8, 9].

The objective of the present paper is to extend the SFBIM to biharmonic problems with boundary singularities. For that purpose we have chosen to solve the Newtonian planar stick–slip problem, which is a benchmark Stokes flow problem used to test various numerical methods proposed in the literature for the solution of viscous and non-Newtonian flows, such as the extrudate–swell flow. This concerns the extrusion of a liquid from a slit or an axisymmetric die into the atmosphere. Due to the relaxation of stresses, the fluid swells as it exits the die. Swelling is particularly pronounced in the case of elastic fluids, but it is also observed in the Newtonian case, provided that the Reynolds number is sufficiently low. The stick–slip problem is a special case of the extrudate–swell problem: in the limit of infinite surface tension, no swelling occurs, and the free surface becomes flat (in the case of slit die). A boundary inverse-square-root stress singularity appears at the exit of the die due to the sudden change of the boundary conditions from the wall to the flat free surface, which is the cause of numerical difficulties that become more severe in the case of non-Newtonian or viscoelastic flows [10, 11].

The creeping planar stick–slip problem was solved analytically by Richardson who used a Wiener–Hopf technique [12] and by Sturges who used the method of matched eigenfunction expansions [13]. Both methods have been used by Trogdon and Joseph [14] to obtain analytical solutions for the round stick–slip problem.

Direct estimates of the leading singular coefficients in the case of the planar stick–slip problem have been reported by various researchers who employed a variety of numerical methods and techniques to incorporate the leading terms of the local asymptotic solution (which is equivalent to subtracting the leading terms of the singularity). Kelmanson employed a direct modified boundary integral equation method (BIEM) incorporating a subtraction of the singular terms technique that accelerated the rate of convergence, and reported estimates for the leading four coefficients [15]. Estimates for these coefficients have also been reported by Georgiou *et al.* [16] who solved the problem using the integrated singular basis function method (ISBFM). In this method, the singular functions are directly subtracted from the original problem formulation which leads to a modified problem with the regular part of the solution and the singular coefficients as unknowns. The smooth problem is then solved using finite elements. The integrals involving singular contributions are reduced to boundary ones by means of a double integration by parts and the original essential boundary conditions are enforced by means of Lagrange multipliers. These two features are encountered also with the SFBIM that we propose in the present work. However, the two methods are quite different

for the following reasons:

(a) With the ISBFM the problem is formulated in terms of the two velocity components and the pressure, while with the SFBIM it is formulated in terms of the streamfunction.
(b) In the ISBFM the unknown fields are the smooth parts of the primary variables which are approximated by means of standard polynomial basis functions. In the SFBIM, however, there is no subtraction of the singularity and the unknown field, i.e. the stream function, is approximated as a linear combination of the leading terms of the local asymptotic expansion. It is clear that such an approximation is valid only if the domain of the problem falls within the domain of convergence of the local solution.
(c) In the ISBFM, the discretized equations are double integrals, whereas in the SFBIM, these are boundary ones. Hence, the dimension of the problem is reduced by one, and the computational cost of the SFBIM is considerably lower than that of the ISBFM.

Karageorghis [17] obtained direct estimates of the first four singular coefficients using a modified method of fundamental solutions (MFS) that was based on the direct subtraction of the leading terms of the singular local solution. A similar method was also used by Poullikkas *et al.* [18] who subtracted only the leading term of the singular local solution assuming that its form is unknown and part of the problem.

Georgiou *et al.* [19] developed a singular finite element method (SFEM), in which special elements incorporating the radial form of the local singularity expansion are employed in a small region around the singular point, in order to resolve the convergence difficulties and improve the accuracy of the global solution. They obtained more accurate results than those achieved with ordinary elements and calculated the leading singular coefficients by post-processing the finite element solution. A similar post-processing technique has been employed by Salamon *et al.* [20] who obtained accurate results near the singularity using high resolution finite elements with quasi-orthogonal mesh generation and local, adaptive mesh refinement with irregular imbedded elements. Ngamaramvaranggul and Webster [21] developed a semi-implicit Taylor–Galerkin/pressure-correction finite element method (STGFEM) for free surface flows and applied it to various Newtonian flows including the plane and axisymmetric stick–slip and extrudate–swell problems. More recently, Normandin *et al.* [22] solved the Newtonian stick–slip problem using a finite element Galerkin technique associated with stream-tube analysis and presented comparisons of the computed streamlines with previous results.

The stick–slip flow of non-Newtonian and viscoelastic fluids has also received considerable attention due to the convergence difficulties associated with the presence of the singularity and the relevance to the extrudate–swell problem. We discuss briefly the literature with emphasis on works reporting results for the Newtonian case. Tanner and Huang [10] applied the *J*-integral method for solving the planar stick–slip flow of power-law fluids, corrected the numerical estimate of singularity strength in Richardson's Newtonian analysis [12], and calculated the first singular coefficient for various power-law exponents. Owens and Phillips [23] presented solutions of the planar stick–slip problem obtained with a spectral domain decomposition method (DDM) for an Oldroyd-B fluid. In a subsequent article, they applied an algebraic mapping to treat the flow domain without truncation and computed the singular coefficients using a post-processing technique [24]. Baaijens investigated the numerical stability of a discontinuous Galerkin method using a Phan–Thien–Tanner model incorporating monotonicity enforcement [25] and applied low-order discontinuous Galerkin methods to solve the

planar stick–slip problem using the Phan–Thien–Tanner and the Maxwell model [11]. More recently, Ngamaramvaranggul and Webster used a Taylor–Galerkin/pressure-correction method with consistent streamline upwinding and velocity gradient recovery to solve the axisymmetric stick–slip flow for an Oldroyd-B flow [26].

The rest of the paper is organized as follows: in Section 2, the Newtonian planar stick–slip problem is introduced and the governing equations and the local asymptotic solution expansion are presented. The SFBIM is developed in Section 3, where four different formulations of the method corresponding to different techniques of imposing the Dirichlet boundary conditions are presented. The numerical results are given in Section 4, where the fast convergence of the method with respect to the number of singular functions is demonstrated and comparisons are made with the the analytical solution [12] and the results obtained with the boundary integral equation method of Kelmanson [15], the spectral domain decomposition method of Owens and Phillips [24], the high-resolution finite element method of Salamon *et al.* [20], the STGFEM of Ngamaramvaranggul and Webster [21], and other methods. The conclusions are summarized in Section 5.

2. GOVERNING EQUATIONS AND ASYMPTOTIC SOLUTION

The planar stick–slip problem is the idealization of the extrusion of a Newtonian fluid between parallel plates at infinite surface tension. The geometry of the flow is depicted in Figure 1. Due to symmetry, only the upper half of the flow domain is considered, i.e. boundary part S_D denotes the plane of symmetry. Boundary parts S_A and S_B represent the wall and the flat free surface, respectively. The latter is flat in the limit of infinite surface tension. Finally, S_C and S_E are, respectively, the artificial inlet and outlet boundaries.

In the creeping case, the flow is governed by the biharmonic equation [27]:

$$\nabla^4 \psi = 0 \quad \text{in } \Omega \tag{1}$$

where ψ is the streamfunction defined by

$$u_x \equiv \frac{\partial \psi}{\partial y} \quad \text{and} \quad u_y \equiv -\frac{\partial \psi}{\partial x} \tag{2}$$

u_x and u_y being the velocity components in the x and y directions, respectively.

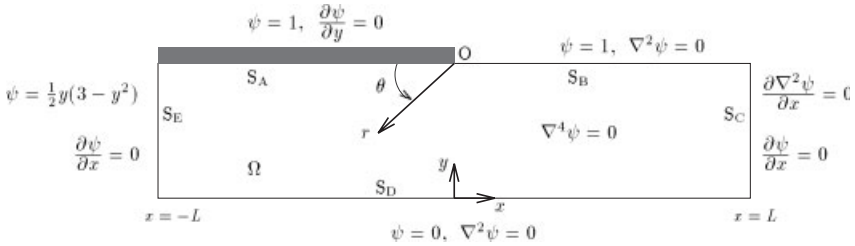

Figure 1. The planar stick–slip problem in terms of the streamfunction ψ.

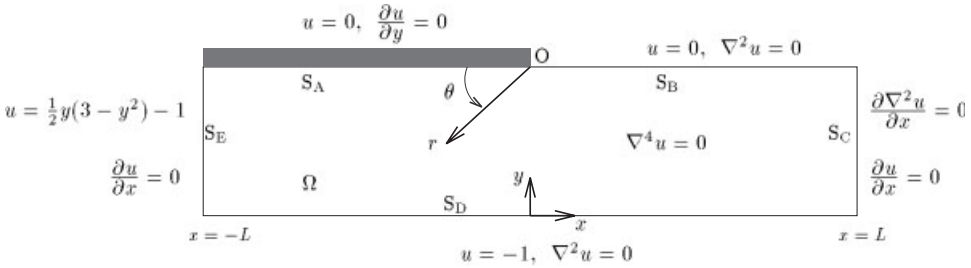

Figure 2. The modified planar stick–slip problem in terms of $u = \psi - 1$.

The boundary conditions of the flow are also depicted in Figure 1. Along the wall S_A there is no slip and no penetration (i.e. the two velocity components are zero). Along the free surface, both u_y and the xy-stress component are zero which leads to $\nabla^2\psi = 0$. The inflow and outflow planes are taken at a distance L before and after the die exit. This distance is assumed to be sufficiently large so that the flow corresponds to the fully developed Poiseuille flow at the inflow plane and to a plug (i.e. uniform) flow at the outflow plane. Finally, along the symmetry plane, the vertical velocity component and the shear stress are zero, i.e. the centreline is a slip surface. The stick–slip flow is characterized by the presence of a stress singularity at the exit O caused by the sudden change in the boundary conditions, from no slip (stick) along the wall S_A to full slip along the flat free surface S_B.

After using the transformation $\psi = u + 1$, the problem of Figure 1 is transformed as follows [23]:

$$\nabla^4 u = 0 \quad \text{in } \Omega \tag{3}$$

with

$$\begin{gathered} u = 0, \quad \frac{\partial u}{\partial y} = 0 \quad \text{on } S_A \\ u = 0, \quad \nabla^2 u = 0 \quad \text{on } S_B \\ \frac{\partial \nabla^2 u}{\partial x} = 0, \quad \frac{\partial u}{\partial x} = 0 \quad \text{on } S_C \\ u = -1, \quad \nabla^2 u = 0 \quad \text{on } S_D \\ u = \tfrac{1}{2}\, y(3 - y^2) - 1, \quad \frac{\partial u}{\partial x} = 0 \quad \text{on } S_E \end{gathered} \tag{4}$$

The transformed problem is also shown in Figure 2. Note that the weak condition

$$\frac{\partial(\nabla^2 u)}{\partial x} = 0 \tag{5}$$

along S_C can be replaced by the stronger Dirichlet condition

$$u = y - 1 \tag{6}$$

which leads to a different formulation, since with the SFBIM, imposing Dirichlet conditions requires the introduction of (unknown) Lagrange multipliers.

The asymptotic solution in the neighbourhood of the singularity can be expressed in terms of an eigenfunction expansion of the form [12, 15, 16]:

$$u(r,\theta)=\sum_{j=1}^{\infty} a_j r^{\mu_j+1} f(\theta,\mu_j), \quad (r,\theta)\in\Omega \tag{7}$$

where (r,θ) are the polar co-ordinates centred at the singular point, μ_j, with $j=1,2,\ldots$, are the singularity powers arranged in ascending order, the functions $f(\theta,\mu_j)$ represent the θ-dependence of the eigensolution, and α_j are the unknown singular coefficients determined by the global flow.

The functions $W^j \equiv r^{\mu_j+1} f(\theta,\mu_j)$ are referred to as singular functions. The local solution (7) consists of even and odd solutions, the corresponding singular functions of which will be denoted by W_1^j and W_2^j, respectively. In the case of even solutions [12],

$$W_1^j \equiv r^{\mu_j+1} f_1(\theta,\mu_j) \tag{8}$$

with

$$f_1(\theta,\mu_j)=\cos(\mu_j+1)\theta-\cos(\mu_j-1)\theta, \quad \mu_j=j-\tfrac{1}{2}, \ j=1,2,\ldots \tag{9}$$

whereas in the case of odd solutions,

$$W_2^j \equiv r^{\mu_j+1} f_2(\theta,\mu_j) \tag{10}$$

with

$$f_2(\theta,\mu_j)=(\mu_j-1)\sin(\mu_j+1)\theta-(\mu_j+1)\sin(\mu_j-1)\theta, \quad \mu_j=j+1, \ j=1,2,\ldots \tag{11}$$

Thus the first singular function is

$$W_1^1=r^{3/2}\left(\cos\frac{3\theta}{2}-\cos\frac{\theta}{2}\right)$$

which indicates that the velocity gradients and the stresses vary as the inverse square root of the radial distance from the singular point.

In what follows we will be using the symbols α_j and β_j for the singular coefficients corresponding to the even and odd singular functions, respectively. Thus, the local solution is written as follows:

$$u=\sum_{j=1}^{\infty}\alpha_j W_1^j+\sum_{j=1}^{\infty}\beta_j W_2^j \tag{12}$$

3. THE SFBIM

In the SFBIM [5] the solution of problem (3)–(4) is approximated by the leading terms of the local solution expansion (12). By employing the first N_α terms in both sums of (12) the approximate solution $\bar{u}$ is

$$\bar{u}=\sum_{j=1}^{N_\alpha}\bar{\alpha}_j W_1^j+\sum_{j=1}^{N_\alpha}\bar{\beta}_j W_2^j \tag{13}$$

where $\bar{\alpha}_j$ and $\bar{\beta}_j$ are the approximations of the singular coefficients. Obviously, the total number of singular functions involved in approximation (13) is $2N_\alpha$.

By applying Galerkin's principle, the governing equation is weighted by the singular functions used in the approximation of the solution. Hence, the following set of discretized equations is obtained:

$$\int_\Omega \nabla^4 \bar{u} W_k^i \, \mathrm{d}V = 0, \quad i = 1, 2, \ldots, N_\alpha, \;\; k = 1, 2 \tag{14}$$

By applying Green's theorem twice and taking into account that the singular functions W_k^i, are biharmonic, the above volume integrals are reduced to boundary ones:

$$\begin{aligned} &\int_{\partial\Omega} \left(\frac{\partial \bar{u}}{\partial n} \nabla^2 W_k^i - \bar{u} \frac{\partial (\nabla^2 W_k^i)}{\partial n} \right) \mathrm{d}S \\ &\quad + \int_{\partial\Omega} \left(\frac{\partial (\nabla^2 \bar{u})}{\partial n} W_k^i - \nabla^2 \bar{u} \frac{\partial W_k^i}{\partial n} \right) \mathrm{d}S = 0, \quad i = 1, 2, \ldots, N_a, \;\; k = 1, 2 \end{aligned} \tag{15}$$

where $\partial\Omega = S_\mathrm{A} \cup S_\mathrm{B} \cup S_\mathrm{C} \cup S_\mathrm{D} \cup S_\mathrm{E}$. The dimension of the problem is, thus, reduced by one, which leads to a considerable reduction of the computational cost. Since W_k^i satisfy exactly the boundary conditions along S_A and S_B, the above integral along these boundary segments, is identically zero. Therefore,

$$\begin{aligned} &\int_{S_\mathrm{C} \cup S_\mathrm{D} \cup S_\mathrm{E}} \left(\frac{\partial \bar{u}}{\partial n} \nabla^2 W_k^i - \bar{u} \frac{\partial (\nabla^2 W_k^i)}{\partial n} \right) \mathrm{d}S + \int_{S_\mathrm{C} \cup S_\mathrm{D} \cup S_\mathrm{E}} \left(\frac{\partial (\nabla^2 \bar{u})}{\partial n} W_k^i - \nabla^2 \bar{u} \frac{\partial W_k^i}{\partial n} \right) \mathrm{d}S = 0, \\ &\quad i = 1, 2, \ldots, N_a, \;\; k = 1, 2 \end{aligned} \tag{16}$$

In the SFBIM the Dirichlet boundary conditions are imposed by means of Lagrange multipliers which replace the normal derivative of the solution u. In the problem under study Dirichlet boundary conditions appear only along boundary parts S_D and S_E. Since along S_E the normal derivative $\partial u / \partial x$ vanishes, Lagrange multipliers are chosen to replace $\partial(\nabla^2 u)/\partial x$ in the boundary integrals of Equation (16). Boundary parts S_D and S_E are partitioned into three-node elements and the corresponding Lagrange multipliers, denoted respectively by λ_D and λ_E, are expanded in terms of quadratic basis functions M^j:

$$\lambda_\mathrm{D} = \frac{\partial \bar{u}}{\partial y} = \sum_{j=1}^{N_{\lambda_\mathrm{D}}} \lambda_\mathrm{D}^j M^j \quad \text{on } S_\mathrm{D} \tag{17}$$

and

$$\lambda_\mathrm{E} = \frac{\partial (\nabla^2 \bar{u})}{\partial x} = \sum_{j=1}^{N_{\lambda_\mathrm{E}}} \lambda_\mathrm{E}^j M^j \quad \text{on } S_\mathrm{E} \tag{18}$$

where N_{λ_D} and N_{λ_E} are the numbers of the discrete Lagrange multipliers λ_D^j and λ_E^j along the corresponding boundaries. The nodal values of λ_D and λ_E are additional unknowns of the problem. The required $N_{\lambda_\mathrm{D}} + N_{\lambda_\mathrm{E}}$ additional equations are obtained by weighting the Dirichlet boundary conditions along S_D and S_E by the quadratic basis functions M^j in the Galerkin

sense. The following linear system of $2N_\alpha + N_{\lambda_D} + N_{\lambda_E}$ discretized equations is thus obtained:

$$\int_{S_C} \left(-\bar{u} \frac{\partial(\nabla^2 W_k^i)}{\partial x} - \nabla^2 \bar{u} \frac{\partial W_k^i}{\partial x} \right) \mathrm{d}y + \int_{S_D} \left(-\lambda_D \nabla^2 W_k^i + \bar{u} \frac{\partial(\nabla^2 W_k^i)}{\partial y} - \frac{\partial(\nabla^2 \bar{u})}{\partial y} W_k^i \right) \mathrm{d}x + \int_{S_E} \left(-\lambda_E W_k^i + \bar{u} \frac{\partial(\nabla^2 W_k^i)}{\partial x} + \nabla^2 \bar{u} \frac{\partial W_k^i}{\partial x} \right) \mathrm{d}y = 0, \quad i = 1, \ldots, N_a, \ k = 1, 2 \tag{19}$$

$$\int_{S_D} \bar{u} M^i \, \mathrm{d}x = -\int_{S_D} M^i \, \mathrm{d}x, \quad i = 1, 2, \ldots, N_{\lambda_D} \tag{20}$$

$$\int_{S_E} \bar{u} M^i \, \mathrm{d}y = \int_{S_E} \left[\frac{1}{2} y(3 - y^2) - 1 \right] M^i \, \mathrm{d}y, \quad i = 1, 2, \ldots, N_{\lambda_E} \tag{21}$$

The above linear system is not symmetric. This can be written in block form as follows:

$$\begin{bmatrix} K & K'_D & K_E \\ K''_D & O & O \\ K_E^T & O & O \end{bmatrix} \begin{bmatrix} X_{\bar{\alpha}, \bar{\beta}} \\ \Lambda_D \\ \Lambda_E \end{bmatrix} = \begin{bmatrix} O \\ B \\ C \end{bmatrix} \tag{22}$$

where $X_{\bar{\alpha}, \bar{\beta}}$, Λ_D and Λ_E are the vectors of the unknowns:

$$X_{\bar{\alpha}, \bar{\beta}} = [\bar{\alpha}_1, \ldots, \bar{\alpha}_{N_\alpha}, \bar{\beta}_1, \ldots, \bar{\beta}_{N_\alpha}]^T$$

$$\Lambda_D = [\lambda_D^1, \lambda_D^2, \ldots, \lambda_D^{N_{\lambda_D}}]^T$$

$$\Lambda_E = [\lambda_E^1, \lambda_E^2, \ldots, \lambda_E^{N_{\lambda_E}}]^T$$

It should be noted that the integrands in the above equations are non-singular and all integrations are carried out far from the boundaries causing the singularity. Note that the stiffness matrix is not symmetric and that it becomes singular if $N_\lambda > 2N_\alpha$ where $N_\lambda = N_{\lambda_D} + N_{\lambda_E}$. The above formulation will be referred to as Formulation A. We have also considered three alternative formulations which are briefly discussed below.

3.1. Formulation B

The only difference between this formulation and Formulation A is that function λ_D along boundary part S_D replaces the normal derivative of the Laplacian of u:

$$\lambda_D = \frac{\partial(\nabla^2 \bar{u})}{\partial y} = \sum_{j=1}^{N_{\lambda_D}} \lambda_D^j M^j \quad \text{on } S_D \tag{23}$$

instead of the normal derivative of u. Therefore, the only change in the formulation is in the boundary integral along the centreline plane, S_D, which becomes:

$$\int_{S_D} \left(-\lambda_D W_k^i + \bar{u} \frac{\partial(\nabla^2 W_k^i)}{\partial y} - \frac{\partial \bar{u}}{\partial y} \nabla^2 W_k^i \right) \mathrm{d}x$$

In contrast to formulation A, the resulting linear system of equations is symmetric. As before the stiffness matrix is singular if $N_\lambda > 2N_\alpha$.

3.2. Formulation C

In this formulation, the weak boundary condition $\partial \nabla^2 u / \partial x = 0$ along S_C is replaced by

$$u = y - 1 \quad \text{on } S_C \tag{24}$$

The use of this essential boundary condition requires the introduction of an additional Lagrange multiplier function, λ_C, which replaces the normal derivative of the Laplacian of u and is expressed in terms of quadratic basis functions M^j:

$$\lambda_C = \frac{\partial(\nabla^2 \bar{u})}{\partial x} = \sum_{j=1}^{N_{\lambda_C}} \lambda_C^j M^j \quad \text{on } S_C \tag{25}$$

As is the case with the other essential boundary conditions, condition (24) is weighted by means of the basis functions M^j. A linear system of $2N_\alpha + N_{\lambda_C} + N_{\lambda_D} + N_{\lambda_E}$ equations is thus obtained:

$$\begin{aligned}
&\int_{S_C} \left(\lambda_C W_k^i - \bar{u} \frac{\partial(\nabla^2 W_k^i)}{\partial x} - \nabla^2 \bar{u} \frac{\partial W_k^i}{\partial x} \right) \mathrm{d}y \\
&+ \int_{S_D} \left(-\lambda_D \nabla^2 W_k^i + \bar{u} \frac{\partial(\nabla^2 W_k^i)}{\partial y} - \frac{\partial(\nabla^2 \bar{u})}{\partial y} W_k^i \right) \mathrm{d}x \\
&+ \int_{S_E} \left(-\lambda_E W_k^i + \bar{u} \frac{\partial(\nabla^2 W_k^i)}{\partial x} + \nabla^2 \bar{u} \frac{\partial W_k^i}{\partial x} \right) \mathrm{d}y = 0, \quad i = 1, \ldots, N_a, \ k = 1, 2
\end{aligned} \tag{26}$$

$$\int_{S_C} \bar{u} M^i \, \mathrm{d}y = \int_{S_C} (y - 1) M^i \, \mathrm{d}y, \quad i = 1, 2, \ldots, N_{\lambda_C} \tag{27}$$

$$\int_{S_D} \bar{u} M^i \, \mathrm{d}x = -\int_{S_D} M^i \, \mathrm{d}x, \quad i = 1, 2, \ldots, N_{\lambda_D} \tag{28}$$

$$\int_{S_E} \bar{u} M^i \, \mathrm{d}y = \int_{S_E} \left[\frac{1}{2} y(3 - y^2) - 1 \right] M^i \, \mathrm{d}y, \quad i = 1, 2, \ldots, N_{\lambda_E} \tag{29}$$

The above linear system is not symmetric. The stiffness matrix is singular if $N_\lambda > 2N_\alpha$ where here $N_\lambda = N_{\lambda_C} + N_{\lambda_D} + N_{\lambda_E}$.

3.3. Formulation D

As in Formulation B, the Lagrange multiplier function λ_D, used to impose the Dirichlet boundary conditions along S_D, replaces the normal derivative of the Laplacian of u (Equation (23)). The resulting linear system of discretized equations is the same as that of Formulation C except from the integral along S_D in Equation (25), which becomes:

$$\int_{S_D} \left(-\lambda_D W_k^i + \bar{u} \frac{\partial(\nabla^2 W_k^i)}{\partial y} - \frac{\partial \bar{u}}{\partial y} \nabla^2 W_k^i \right) \mathrm{d}x$$

As in formulation B, the system of the discretized equations is symmetric.

4. NUMERICAL RESULTS

Calculations have been carried out with all four formulations presented in Section 3. In order to implement the SFBIM, the boundary parts S_C, S_D and S_E (i.e. the boundary parts away from the singularity) are subdivided into quadratic elements. Specifically, we employ N_E elements over each one of boundaries S_E, S_C and N_D elements over boundary S_D. Thus, the total number of Lagrange multipliers in formulations A and B is $N_\lambda = N_{\lambda_E} + N_{\lambda_D}$ and in formulations C and D is $N_\lambda = N_{\lambda_C} + N_{\lambda_D} + N_{\lambda_E} = 2N_{\lambda_E} + N_{\lambda_D}$ (where $N_{\lambda_E} = 2N_E + 1$ and $N_{\lambda_D} = 2N_D + 1$). As in Reference [5], the integrals in all formulations are calculated numerically by subdividing each quadratic element into 10 subintervals and using a 15-point Gauss–Legendre quadrature over each subinterval. Unless otherwise indicated, the semi-length L of the domain has been taken equal to 3.

As already mentioned, the number of the singular functions $2N_\alpha$ should be much greater than the number of Lagrange multipliers N_λ, since otherwise the stiffness matrix is ill-conditioned or singular. On the other hand, large values of $2N_\alpha$ should be avoided because the contributions of the high-order singular functions become either negligible (for $r<1$) or very large (for $r>1$) beyond the limits double precision can handle.

Systematic runs have been carried out in order to study the effects of both N_α and N_λ on the numerical results. The effect of $2N_\alpha$ on the leading singular coefficients can be observed in Tables I and II, which show results obtained using formulation A with $N_\lambda = 32$. Fast convergence is observed as $2N_\alpha$ is increased and accurate estimates of the leading singular coefficients are obtained. However, at very high values of $2N_\alpha$ (i.e. above $2N_\alpha = 88$) slow divergence is observed due to the inaccuracies introduced by the high-order singular functions.

The convergence of the method with the number of Lagrange multipliers is shown in Tables III and IV which show the values of the leading singular coefficients calculated with $2N_\alpha = 88$ and various values of $N_\lambda = N_{\lambda_D} + N_{\lambda_E}$. Again, fast convergence is observed initially but as N_λ approaches the value of $2N_\alpha$, the results start diverging slowly, which is attributed to the fact that the stiffness matrix becomes ill-conditioned. Our computations showed that the optimal values of N_λ and $2N_\alpha$ are $N_\lambda = 32$ and $2N_\alpha = 88$. For higher values of $2N_\alpha$ (e.g. $2N_\alpha = 120$) satisfactory values of the singular coefficients are still obtained, but the quality of the global solution is not very good.

An indication of the quality of the solution is given by the smoothness of the calculated Lagrange multipliers. Thus, for the optimal combination $N_\lambda = 32$ and $2N_\alpha = 88$ with formulation A, the calculated Lagrange multiplier function along boundary S_D is smooth. As shown in

Table I. Convergence of the leading singular coefficients α_i with $2N_\alpha$; $N_\lambda = 32$, formulation A.

$2N_\alpha$	α_1	α_2	α_3	α_4	α_5	α_{10}
70	0.6909892	0.2645003	0.030364	−0.021405	−0.002845	0.00024
80	0.6909881	0.2645007	0.030376	−0.021407	−0.002900	0.00022
86	0.6909882	0.2645004	0.030374	−0.021405	−0.002892	0.00021
88	0.6909882	0.2645004	0.030374	−0.021404	−0.002891	0.00021
90	0.6909882	0.2645002	0.030375	−0.021403	−0.002895	0.00021
92	0.6909885	0.2645045	0.030371	−0.021436	−0.002875	0.00034
100	0.6909884	0.2644998	0.030371	−0.021401	−0.002878	0.00020
110	0.6909883	0.2645004	0.030374	−0.021405	−0.002891	0.00021
120	0.6909883	0.2645003	0.030374	−0.021404	−0.002890	0.00021
130	0.6909882	0.2645003	0.030375	−0.021404	−0.002897	0.00020
140	0.6909873	0.2644989	0.030387	−0.021393	−0.002943	0.00019
150	0.6909883	0.2645008	0.030373	−0.021407	−0.002886	0.00021

Table II. Convergence of the leading singular coefficients β_i, with $2N_\alpha$; $N_\lambda = 32$, formulation A.

$2N_\alpha$	β_1	β_2	β_3	β_4	β_5	β_{10}
70	−0.0808635	−0.017115	0.001726	0.001231	−0.000282	−0.000001
80	−0.0808617	−0.017119	0.001720	0.001240	−0.000270	−0.000006
86	−0.0808619	−0.017119	0.001720	0.001238	−0.000271	−0.000005
88	−0.0808619	−0.017119	0.001720	0.001238	−0.000271	−0.000005
90	−0.0808617	−0.017119	0.001720	0.001238	−0.000270	−0.000005
92	−0.0808645	−0.017122	0.001729	0.001245	−0.000287	−0.000009
100	−0.0808621	−0.017117	0.001721	0.001234	−0.000273	−0.000003
110	−0.0808619	−0.017119	0.001720	0.001238	−0.000272	−0.000005
120	−0.0808619	−0.017118	0.001720	0.001237	−0.000271	−0.000005
130	−0.0808617	−0.017119	0.001720	0.001239	−0.000270	−0.000006
140	−0.0808590	−0.017121	0.001711	0.001231	−0.000258	−0.000008
150	−0.0808623	−0.017119	0.001721	0.001237	−0.000273	−0.000005

Figure 3(a), for a slightly different value of N_λ (i.e. $N_\lambda = 36$), the calculated Lagrange multiplier function exhibits oscillations, while the values of the singular coefficients are essentially the same. Similar observations are made in Figures 3(b)–(d) with the results of formulations B–D. Recall here that in formulations A and C, λ_D replaces $\partial u/\partial y$ while in formulations B and D it replaces $\partial(\nabla^2 u)/\partial y$. From the results of Figure 3, it is clear that formulations A and C are more stable. Since it does not require additional Lagrange multipliers along boundary S_C, formulation A is to be preferred. The converged values of the leading singular coefficients with all formulations are depicted in Table V. Note the slight differences in the values of $2N_\alpha$ and N_λ required for convergence. In Table VI, the values of α_1, α_2, α_3 and β_1, calculated using formulation A, are compared with values reported in the literature. To our knowledge, there are no reports in the literature for the values of the higher-order coefficients. The value 0.690988 for α_1 agrees with the analytical solution up to the sixth significant digit and is much more accurate than previously reported values. The values of the other three coefficients

Table III. Convergence of the leading singular coefficients α_i with N_λ; $2N_\alpha = 88$, formulation A.

$N_\lambda = N_{\lambda_D} + N_{\lambda_E}$	α_1	α_2	α_3	α_4	α_5	α_{10}
$13+5$	0.6909940	0.2645260	0.030339	−0.021474	−0.002801	0.00041
$17+7$	0.6909864	0.2644962	0.030396	−0.021382	−0.002969	0.00019
$21+5$	0.6909883	0.2645002	0.030374	−0.021403	−0.002890	0.00021
$21+7$	0.6909882	0.2645007	0.030375	−0.021407	−0.002893	0.00022
$25+5$	0.6909883	0.2645002	0.030373	−0.021403	−0.002888	0.00021
$25+7$	0.6909882	0.2645004	0.030374	−0.021404	−0.002891	0.00021
$25+9$	0.6909882	0.2645005	0.030375	−0.021405	−0.002895	0.00021
$29+7$	0.6909883	0.2645002	0.030374	−0.021403	−0.002892	0.00021
$29+9$	0.6909882	0.2645005	0.030374	−0.021405	−0.002892	0.00021
$33+7$	0.6909883	0.2645004	0.030338	−0.021427	−0.002707	0.00039
$33+9$	0.6909876	0.2645077	0.030435	−0.021461	−0.003168	0.00048

Table IV. Convergence of the leading singular coefficients β_i with N_λ; $2N_\alpha = 88$, formulation A.

$N_\lambda = N_{\lambda_D} + N_{\lambda_E}$	β_1	β_2	β_3	β_4	β_5	β_{10}
$13+5$	−0.0808768	−0.017123	0.001747	0.001248	−0.000307	−0.000018
$17+7$	−0.0808566	−0.017121	0.001706	0.001243	−0.000251	−0.000008
$21+5$	−0.0808618	−0.017118	0.001720	0.001237	−0.000271	−0.000005
$21+7$	−0.0808620	−0.017119	0.001721	0.001239	−0.000272	−0.000006
$25+5$	−0.0808619	−0.017118	0.001720	0.001237	−0.000271	−0.000005
$25+7$	−0.0808619	−0.017119	0.001720	0.001238	−0.000271	−0.000005
$25+9$	−0.0808618	−0.017119	0.001720	0.001239	−0.000271	−0.000006
$29+7$	−0.0808618	−0.017118	0.001720	0.001237	−0.000271	−0.000005
$29+9$	−0.0808619	−0.017119	0.001720	0.001238	−0.000271	−0.000005
$33+7$	−0.0808654	−0.017109	0.001747	0.001215	−0.000324	−0.000009
$33+9$	−0.0808571	−0.017146	0.001700	0.001303	−0.000237	−0.000049

compare well with numerical results reported in the literature, especially with those calculated by the spectral domain decomposition method of Owens and Phillips [24].

Once the streamfunction is known, the two velocity components are directly calculated by means of Equation (2). Plots of the axial velocity, u_x, along the slip surface ($y = 1$) and the centreline ($y = 0$), computed using formulation A with $2N_\alpha = 88$ and $N_\lambda = 32$, are shown in Figure 4. The calculated slip surface velocity is in good agreement with the predictions of Kelmanson [15] and Owens and Phillips [24], while the centreline velocity agrees very well with the high-resolution finite element predictions of Salamon *et al.* [20], which is also indicated in Table VII, where the values of u_x at three points of the domain are compared. A comparison against the analytical solution along the symmetry plane (as calculated by Ngamaramvaranggul and Webster [21]) is provided in Table VIII. The small differences observed are due to the fact that the domain used by Richardson [12] was shorter ($L = 2$). However, the predictions of the present method are still much closer to the analytical solution than those of the STGFEM of Ngamaramvaranggul and Webster [21]. Finally, as illustrated in Table IX, the calculated value of u_x at (0.2,1) compares well with the analytical solution (based on the graphical information recorded in Reference [12]), and is better than the

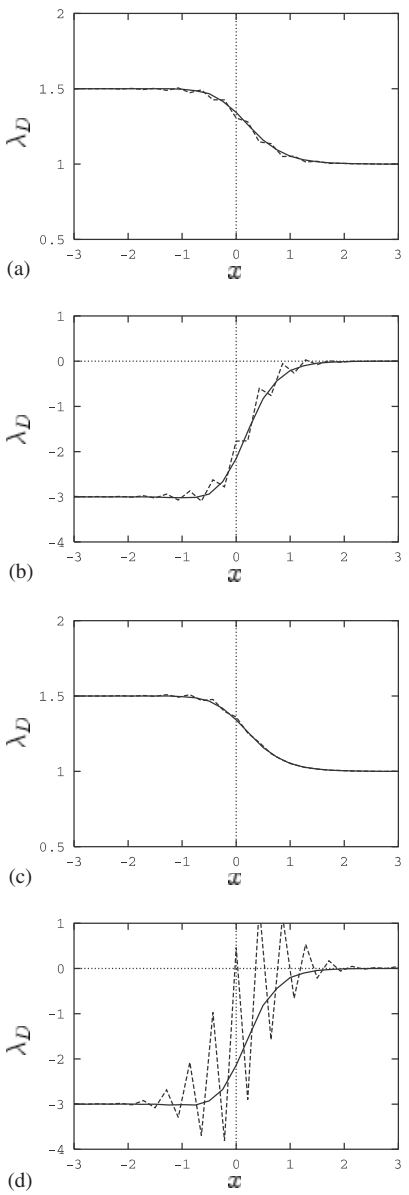

Figure 3. Converged (solid) and oscillatory (dashed) Lagrange multiplier functions along boundary S_D calculated with formulations A–D. (a) Formulation A: $N_\lambda = 32$ (solid) and 36 (dashed) $2N_\alpha = 88$; (b) Formulation B: $N_\lambda = 32$ (solid) and 36 (dashed) $2N_\alpha = 90$; (c) Formulation C: $N_\lambda = 39$ (solid) and 43 (dashed) $2N_\alpha = 90$; and (d) Formulation D: $N_\lambda = 39$ (solid) and 43 (dashed) $2N_\alpha = 90$.

Table V. Converged values of singular coefficients with formulations A–D.

Singular coefficient	Formulation A $2N_\alpha = 88,\ N_\lambda = 32$	Formulation B $2N_\alpha = 90,\ N_\lambda = 32$	Formulation C $2N_\alpha = 90,\ N_\lambda = 39$	Formulation D $2N_\alpha = 90,\ N_\lambda = 39$
α_1	0.690988	0.690988	0.690989	0.690989
α_2	0.264500	0.264500	0.264500	0.264500
α_3	0.03037	0.03037	0.03037	0.03037
α_4	−0.02140	−0.02140	−0.02140	−0.02140
α_5	−0.00289	−0.00289	−0.00289	−0.00289
α_6	0.00423	0.00423	0.00423	0.00423
α_7	0.00042	0.00041	0.00041	0.00041
α_8	−0.00093	−0.00093	−0.00093	−0.00093
α_9	−0.00007	−0.00007	−0.00007	−0.00007
α_{10}	0.0002	0.0002	0.0002	0.0002
β_1	−0.080862	−0.080862	−0.080862	−0.080862
β_2	−0.017119	−0.017118	−0.017119	−0.017118
β_3	0.00172	0.00172	0.00172	0.00172
β_4	0.00124	0.00124	0.00124	0.00124
β_5	−0.00027	−0.00027	−0.00027	−0.00027
β_6	−0.00017	−0.00017	−0.00017	−0.00017
β_7	0.00005	0.00005	0.00005	0.00005
β_8	0.00003	0.00003	0.00003	0.00003
β_9	−0.00001	−0.00001	−0.00001	−0.00001
β_{10}	0.00000	0.00000	0.00000	0.00000

Table VI. Comparison of computed singular coefficients (formulation A with $2N_\alpha = 88$ and $N_\lambda = 32$) with the results of other numerical methods.

Method	α_1	α_2	α_3	β_1
Modified BIEM* [15]	0.69108	0.26435	0.04962	−0.07990
Singular FEM† [19]	0.69173	0.27168	0.05013	
ISBFM [16]	0.69104	0.26140	−0.01263	
Modified MFS [17]	0.690984	0.274807	−0.022104	−0.043983
J-integral method [10]	0.6910			
Spectral DDM† [24]	0.69035	0.26404	0.03069	−0.08051
High-resolution FEM† [20]	0.69160	0.27183	0.05232	
Modified MFS‡ [18]	0.69019			
SFBIM (present work)	0.690988	0.264500	0.03037	−0.080862
Analytical solution [12]	0.6909883			

* Extrapolated values.
† Singular coefficients obtained by post-processing the numerical solution.
‡ The best reported estimate is listed.

singular boundary element (SBEM) solution of Ingham and Kelmanson [28], the SFEM and ISBFM results of Georgiou *et al.* [16, 19] (as calculated by Ngamaramvaranggul and Webster [21]), and the STGFEM result [21]. It should be noted that Ngamaramvaranggul and Webster [21] used an incorrect value for the analytical solution (0.618040 instead of 0.572).

The pressure corresponding to the local solution (12) is given by [27]

$$p(x, y) = p_1(x, y) - p_0 \tag{30}$$

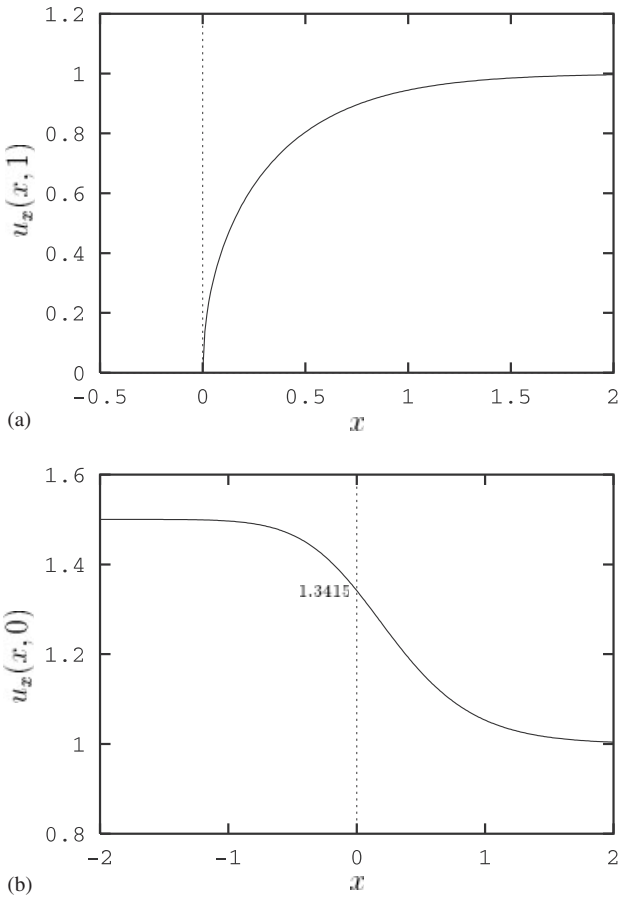

Figure 4. Calculated axial velocity: (a) along the slip surface ($y = 1$); and (b) along the centreline ($y = 0$); formulation A with $2N_\alpha = 88$ and $N_\lambda = 32$.

Table VII. Comparison of computed axial velocities (formulation A with $2N_\alpha = 88$ and $N_\lambda = 32$) with the high-resolution finite element predictions of Salamon *et al.* [20].

	$u_x(0, 0.975)$	$u_x(0, 0)$	$u_x(1, 1)$
Salamon *et al.* [20]	0.234855	1.34150	0.944542
Present work	0.234840	1.34151	0.944528

where

$$p_1 = -4\left[\sum_{j=1}^{\infty}\left(j-\frac{1}{2}\right)\alpha_j r^{j-(3/2)}\sin\left(j-\frac{3}{2}\right)\theta - \sum_{j=1}^{\infty}(j+1)(j+2)\beta_j r^j\cos(j\theta)\right] \tag{31}$$

Table VIII. Computed velocities along the symmetry plane (formulation A, $2N_\alpha = 88$, $N_\lambda = 32$) compared with other results in the literature.

x	Analytical [12]	STGFEM [21]	SFBIM
−1.0	1.4964	1.4959	1.4965
−0.8	1.4899	1.4892	1.4903
−0.6	1.4758	1.4749	1.4766
−0.4	1.4484	1.4479	1.4499
−0.2	1.4027	1.4035	1.4051
0.2	1.2798	1.2701	1.2665
0.4	1.1967	1.2006	1.1929
0.6	1.1308	1.1403	1.1310
0.8	1.0834	1.0996	1.0848
1.0	1.0516	1.0702	1.0530

Table IX. Velocity results at $x = 0.2$ on the slip surface.

Method	Velocity
Analytical [12]	0.572
SBEM [28]	0.572608
SFEM [19]	0.571896
ISBFM [16]	0.571259
STGFEM [21]	0.619786
SFBIM	0.571958

Table X. Variation of the value of $p(0^-, 1)$ with the semi-length L of the domain; formulation A with $2N_\alpha = 88$ and $N_\lambda = 32$.

L	$p(0^-, 1)$
2.0	1.3452
2.2	1.3454
2.4	1.3454
2.6	1.3468
2.8	1.3451
3.0	1.3454
3.2	1.3444
3.4	1.3454

and $p_0 = p(L, 1)$ so that the pressure at $(L, 1)$ is zero. It is clear that the pressure p is at most as accurate as p_0, the accuracy of which deteriorates as the semi-length L of the domain increases, given that the contributions of the singular functions become larger. This effect is illustrated in Table X, where we show the variation of $p(0^-, 1)$ with L. Note that $p_1(0^-, 1) = 0$ and thus

$$p(0^-, 1) = -p_0 = -p(L, 1)$$

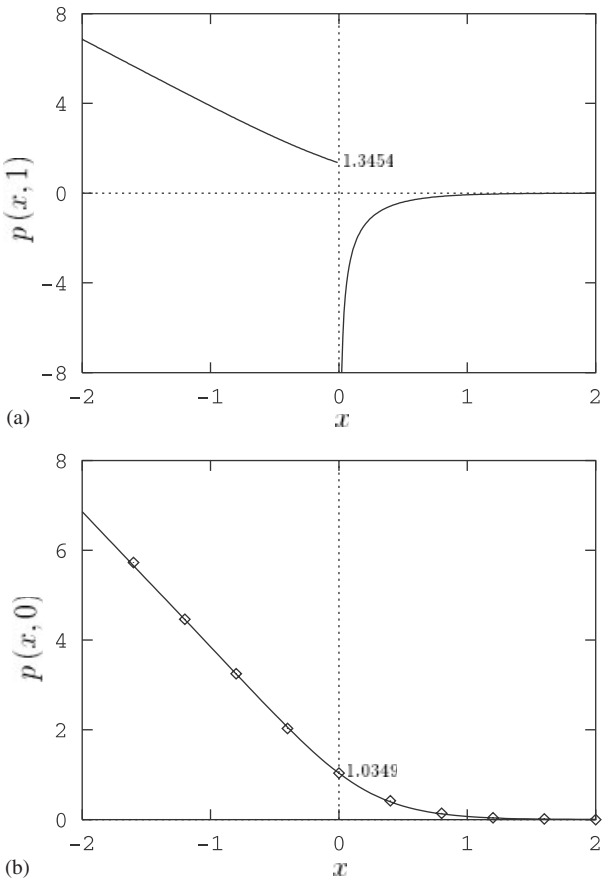

Figure 5. (a) Calculated pressure along $y = 1$; and (b) calculated centreline pressure (continuous curve) compared with the analytical results by Richardson (points) [12]; formulation A with $2N_\alpha = 88$ and $N_\lambda = 32$.

Table XI. Comparison of the computed centreline pressure at $x = 0$ (formulation A with $2N_\alpha = 88$ and $N_\lambda = 32$) with the results of other numerical methods.

Method	$p(0,0)$
Finite differences [29]	1.100
STGFEM [21]	0.9980
SFBIM (present work)	1.0349
Analytical solution [12]	1.0348

In Figure 5(a), the pressure along the wall and the slip surface ($y = 1$) is plotted. This is in good agreement with the results of Salamon *et al.* [20]. Due to the singularity, the pressure goes to minus infinity as the die exit is approached from the right, while it remains finite

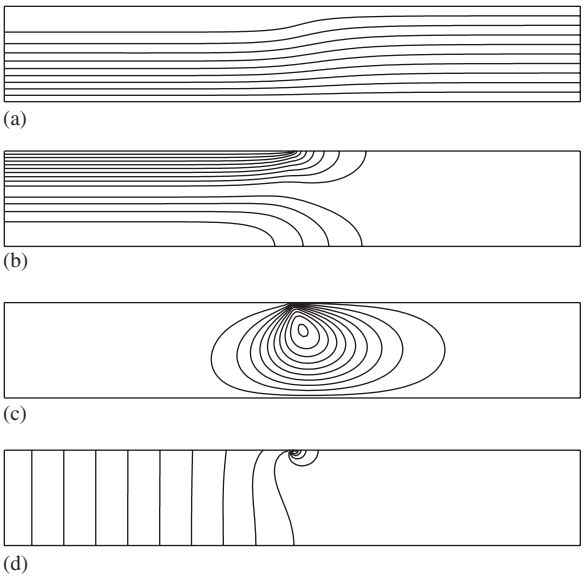

Figure 6. Computed streamlines and contours of the two velocity components and the pressure; formulation A with $2N_\alpha = 88$ and $N_\lambda = 32$. (a) Stream-function, ψ; (b) horizontal velocity component, $u_x = \partial\psi/\partial y$; (c) vertical velocity component, $u_y = -\partial\psi/\partial x$; and (d) pressure, p.

Table XII. Converged values of the leading singular coefficients with formulation A, $N_\lambda = 32$ and different values of the semi-length L of the domain; the value of $2N_\alpha$ ranges from 78 to 88, depending on the value of L.

L	α_1	α_2	β_1	β_2
2.0	0.690973	0.264524	−0.080870	−0.017112
2.1	0.690980	0.264514	−0.080866	−0.017115
2.2	0.690984	0.264508	−0.080864	−0.017117
2.3	0.690986	0.264504	−0.080863	−0.017117
2.4	0.690987	0.264503	−0.080862	−0.017118
2.5	0.690988	0.264502	−0.080862	−0.017118
2.6	0.690988	0.264501	−0.080862	−0.017118
2.7	0.690988	0.264501	−0.080862	−0.017118
2.8	0.690988	0.264501	−0.080862	−0.017118
2.9	0.690988	0.264500	−0.080862	−0.017118
3.0	0.690988	0.264500	−0.080862	−0.017118
3.1	0.690988	0.264500	−0.080862	−0.017118
3.2	0.690988	0.264500	−0.080862	−0.017118
3.3	0.690988	0.264500	−0.080862	−0.017117
3.4	0.690988	0.264500	−0.080862	−0.017118
3.5	0.690988	0.264498	−0.080862	−0.017117
3.6	0.690988	0.264498	−0.080862	−0.017117
3.8	0.690988	0.264498	−0.080862	−0.017118
4.0	0.690988	0.264490	−0.080862	−0.017113

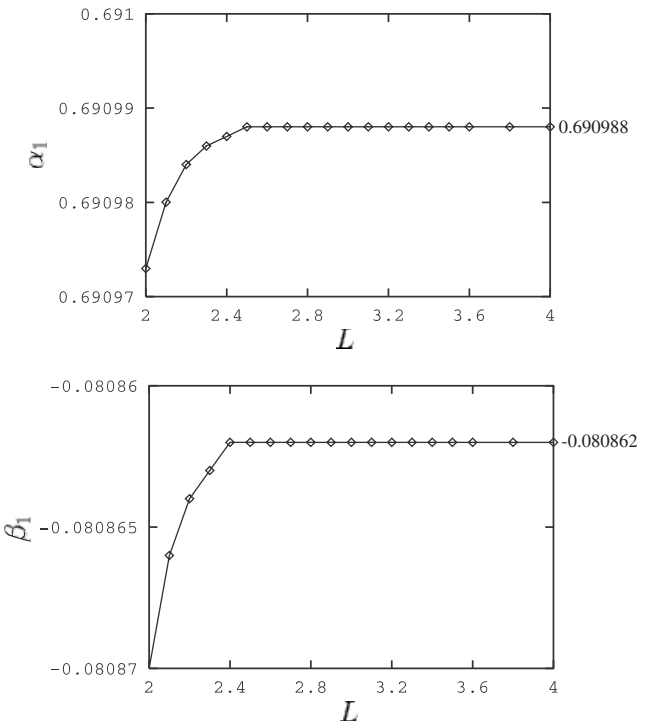

Figure 7. Convergence of α_1 and β_1 with the semi-length L of the domain: formulation A, $N_\lambda = 32$.

(and positive) for negative x. The negative value of the pressure implies that the fluid in the extrudate region is subjected to tension. Note that the discontinuity cannot be captured by standard numerical methods in which a continuous approximation is used for the pressure. In Figure 5(b), the computed centreline pressure is compared with the analytical results of Richardson [12] (as given by Ngamaramvaranggul and Webster [21]). The agreement is excellent, which is also seen in Table XI, where the computed value of $p(0,0)$ is compared with the analytical value and those of other numerical methods.

The streamlines as well as the contours of the two velocity components (u_x and u_y) and the pressure, computed using formulation A with $2N_\alpha = 88$ and $N_\lambda = 32$, are shown in Figure 6. These show the re-adjustment of the flow from a parabolic to a uniform velocity profile and agree well with previous results in the literature [16, 20, 22]. The maximum value of u_y is 0.19364 which compares well with the value of 0.1936 provided by Salamon *et al.* [20]. (Ngamaramvaranggul and Webster [21] computed the peak value to be 0.17.) According to our calculations, the maximum occurs approximately at the point $(0.109, 0.712)$.

The effect of the length of the domain on the computations has also been studied. Table XII depicts the converged values of the first four singular coefficients for $N_\lambda = 32$ and different values of the semi-length, L, of the domain. As expected, the values of the singular coefficients change dramatically with L for small values of the latter, since the assumptions for fully developed and uniform flow along the inlet and outlet planes, respectively, are not valid when the two planes are taken close to the die exit. This effect is illustrated in Figure 7, where

the calculated values of α_1 and β_1 are plotted versus L. We observe that the value $L=3$ is sufficiently high to assure the validity of the imposed inlet and outlet boundary conditions. At higher values of L, the accuracy of the computed solutions starts deteriorating, due to the fact that the number N_{λ_D} of the corresponding Lagrange multipliers is kept fixed while the length of the boundary S_D increases. As already noted, increasing N_{λ_D} will not improve the accuracy, since it leads to ill-conditioning of the stiffness matrix.

5. CONCLUSIONS

The singular function boundary integral method (SFBIM) has been developed for solving a biharmonic problem with a boundary singularity, i.e. the Newtonian planar stick–slip problem in terms of the streamfunction. The solution is approximated by means of the leading singular functions defined by the local asymptotic solution expansion around the singularity. Hence, the method is restricted to Stokes problems with a boundary singularity for which the local solution is available. The proposed approximation is valid only if the domain of the problem is a subset of the domain of convergence of the local solution. If this is not the case, the domain can be partitioned into subdomains over which separate approximations, that obey appropriate compatibility conditions along the interfaces, may be used.

The main features of the SFBIM are as follows:

(a) The singular coefficients are calculated directly.
(b) The governing biharmonic equation is weighted by the singular functions in the Galerkin sense.
(c) The discretized equations are reduced to boundary integrals by means of a double application of the divergence theorem, which leads to a considerable reduction of the computational cost.
(d) The Dirichlet boundary conditions are weakly enforced by means of Lagrange multipliers which may replace either $\partial u/\partial n$ or $\partial(\nabla^2 u)/\partial n$ in the integrands of the discretized equations. The Lagrange multipliers are calculated together with the singular coefficients.

Four different formulations of the SFBIM, corresponding to different techniques of imposing the Dirichlet boundary conditions, have been investigated. Even though all formulations give about the same results, using a weaker instead of a Dirichlet condition along the outflow plane is a much better choice, since the number of Lagrange multipliers, N_λ must be much lower than the number of singular functions, $2N_\alpha$ in order to avoid ill-conditioning of the stiffness matrix. Moreover, the best choice for the Lagrange multipliers along the symmetry plane is to replace the normal derivative of the solution and not the normal derivative of its Laplacian.

The SFBIM converges very fast with the number of singular functions and the number of Lagrange multipliers, and accurate estimates of the leading singular coefficients are obtained. In particular, the value 0.690988 for the leading singular coefficient agrees well with the analytical solution up to the sixth significant digit. The effect of the length of the domain on the values of the leading singular coefficients has also been investigated. Finally, the numerical results for the velocity components and the pressure compare very well with the analytical solution of Richardson [12] and the high-resolution finite element results of Salamon *et al.* [20].

REFERENCES

1. Li Z-C, Lu TT. Singularities and treatments of elliptic boundary value problems. *Mathematical and Computer Modelling* 2000; **31**:97–145.
2. Dosiyev AA. The high accurate block-grid method for solving Laplace's boundary value problem with singularities. *SIAM Journal on Numerical Analysis* 2004; **42**:153–178.
3. Shi J-M, Breuer M, Durst F. A combined analytical-numerical method for treating corner singularities in viscous flow predictions. *International Journal for Numerical Methods in Fluids* 2004; **45**:659–688.
4. Szabó B, Babuška I. *Finite Element Analysis*. Wiley: New York, 1991.
5. Elliotis M, Georgiou G, Xenophontos C. The solution of a Laplacian problem over an L-shaped domain with a singular function boundary integral method. *Communications in Numerical Methods in Engineering* 2002; **18**:213–222.
6. Babuška I, Miller A. The post-processing approach in the finite element method. Part 2: the calculation of stress intensity factors. *International Journal for Numerical Methods in Engineering* 1984; **20**:1111–1129.
7. Szabó BA, Yosibash Z. Numerical analysis of singularities in two dimensions. Part 2: computation of generalized flux/stress intensity factors. *International Journal for Numerical Methods in Engineering* 1996; **39**:409–434.
8. Georgiou GC, Olson LG, Smyrlis Y. A singular function boundary integral method for the Laplace equation. *Communications in Numerical Methods in Engineering* 1996; **12**:127–134.
9. Georgiou GC, Boudouvis A, Poullikkas A. Comparison of two methods for the computation of singular solutions in elliptic problems. *Journal of Computational and Applied Mathematics* 1997; **79**:277–290.
10. Tanner RI, Huang X. Stress singularities in non-Newtonian stick-slip and edge flows. *Journal of Non-Newtonian Fluid Mechanics* 1993; **50**:135–160.
11. Baaijens FPT. Application of low-order discontinuous Galerkin methods to the analysis of viscoelastic flows. *Journal of Non-Newtonian Fluid Mechanics* 1994; **52**:37–57.
12. Richardson S. A stick-slip problem related to the motion of a free jet at low Reynolds numbers. *Proceedings of the Cambridge Philosophical Society* 1970; **67**:477–489.
13. Sturges LD. *Ph.D. Thesis*, University of Minnesota: Minneapolis, 1977.
14. Trogdon SA, Joseph DD. The stick-slip problem for a round jet. I. Large surface tension. *Rheologica Acta* 1980; **19**:404–420.
15. Kelmanson MA. An integral equation method for the solution of singular slow flow problems. *Journal of Computational Physics* 1983; **51**:139–158.
16. Georgiou GC, Olson LG, Schultz WW. The integrated singular basis function method for the stick-slip and the die-swell problems. *International Journal for Numerical Methods in Fluids* 1991; **13**:1251–1265.
17. Karageorghis A. Modified methods of fundamental solutions for harmonic and biharmonic problems with boundary singularities. *Numerical Methods for Partial Differential Equations* 1992; **8**:1–19.
18. Poullikkas A, Karageorghis A, Georgiou G. Methods of fundamental solutions for harmonic and biharmonic boundary value problems. *Computational Mechanics* 1998; **21**:416–423.
19. Georgiou GC, Olson LG, Schultz WW, Sagan S. A singular finite element for Stokes flow: the stick-slip problem. *International Journal for Numerical Methods in Fluids* 1989; **9**:1353–1367.
20. Salamon TR, Bornside DE, Armstrong RC, Brown RA. The role of surface tension in the dominant balance in the die swell singularity. *Physics of Fluids* 1995; **7**:2328–2344.
21. Ngamaramvaranggul V, Webster MF. Computation of free surface flows with a Taylor–Galerkin/pressure-correction algorithm. *International Journal for Numerical Methods in Fluids* 2000; **33**:993–1026.
22. Normandin M, Radu DG, Mahmoud A, Clermont J-R. Finite-element and stream-tube formulations for flow computations—two-dimensional applications. *Mathematics and Computers in Simulation* 2002; **60**:129–134.
23. Owens RG, Phillips TN. A spectral domain decomposition for the planar non-Newtonian stick-slip problem. *Journal of Non-Newtonian Fluid Mechanics* 1991; **41**:43–79.
24. Owens RG, Phillips TN. Mass- and momentum-conserving spectral methods for Stokes flow. *Journal of Computational and Applied Mathematics* 1994; **53**:185–206.
25. Baaijens FPT. Numerical experiments with a discontinuous Galerkin method including monotonicity enforcement on the stick-slip problem. *Journal of Non-Newtonian Fluid Mechanics* 1994; **51**:141–159.
26. Ngamaramvaranggul V, Webster MF. Viscoelastic simulations of stick-slip and die-swell flows. *International Journal for Numerical Methods in Fluids* 2001; **36**:539–595.
27. Papanastasiou T, Georgiou G, Alexandrou A. *Viscous Fluid Flow*. CRC Press: Boca Raton, FL, 1999; 373–386.
28. Ingham DB, Kelmanson MA. *Boundary Integral Equation Analyses of Singular Potential and Biharmonic Problems*. Springer: Berlin, 1984; 21–51.
29. Ahn YC, Ryan ME. A finite difference analysis of the extrudate problem. *International Journal for Numerical Methods in Fluids* 1991; **13**:1289–1310.

